Acta Mech 195, 81–102 (2008)
DOI 10.1007/s00707-007-0544-7
Printed in The Netherlands

Acta Mechanica

*Dedicated to Professor Franz Ziegler on the occasion of his 70th birthday*

# Yield or martensitic phase transformation conditions and dissipation functions for isotropic, pressure-insensitive alloys exhibiting SD effect

**B. Raniecki, Z. Mróz**

Institute of Fundamental Technological Research, Polish Academy of Sciences, Warsaw, Poland

Received 25 September 2007; Accepted 21 November 2007; Published online 15 January 2008


**Summary.** A class of nonsingular yield conditions depending on three parameters is analyzed for isotropic materials exhibiting strength differential effect and pressure insensitivity. The yield condition can then be expressed in terms of the second and third stress deviator invariants. The convexity requirement is considered and the constraints imposed on the material parameters are discussed in detail. The dual dissipation function is derived in the analytical form. The condition can be applied in the analysis of high strength alloys (such as Inconnel 718) or of shape memory alloys (such as NiTi, NiAl, CuZnGa, or CuAlNi) in order to specify the onset of yield, or of martensitic or austenitic transformation. The conditions can easily be generalized to account for mixed hardening and back stress anisotropy. Some experimental data are provided to verify the proposed conditions.

## 1 Introduction

The present work is devoted to the analysis of yield conditions and dissipation potentials for metals or metallic alloys exhibiting the strength differential (SD) effect, namely different yield stress in tension and compression. This effect has been observed in many iron-based metals such as plain carbon or low alloy steels, cast iron and also in some metals such as titanium, aluminium, magnesium and nickel-base super alloys, such as Inconel 718. A separate class of shape memory alloys (NiTi, NiAl, CuZnGa) also exhibit different tensile and compressive critical stresses corresponding to the onset of phase transformation. The corresponding transformation surfaces then exhibit varying critical stresses along radial stress paths.

In early works the SD effect was associated with pressure-dependent flow and dilatancy of metals. Spitzig and Richmond [1] used the Drucker–Prager yield condition dependent on the first stress and the second stress deviator invariants $I_1$, $J_2$ coupled with the associated or non-associated flow rule. The microstructural aspects of SD effect were discussed among others by Chait [2], [3], Casey and Sullivan [4] and Rauch and Leslie [5]. The pressure-dependent dislocation motion was assumed with

Correspondence: Bogdan Raniecki, Institute of Fundamental Technological Research, Polish Academy of Sciences, Świętokrzyska 21, 00-049 Warsaw, Poland
e-mail: braniec@ippt.gov.pl

plastic strain exhibiting volumetric portion. The importance of non-Schmid effects in slip systems was emphasized by Kuroda and Kuwabara [6].

However, for hexagonal close packed (hcp) materials the twinning and slip mechanism contribute to SD effect, cf. Hosford and Allen [7] and Hosford [8]. As these metals are pressure insensitive, the dependence of the yield condition on the first stress invariant should be neglected and the effect of the third stress deviator invariant $J_3$ becomes important. Similarly, the onset of martensitic transformation in shape memory alloys was assumed to depend on $J_3$, cf. Raniecki and Lexcellent [9] and Lexcellent et al. [10], or generated from micromechanical models, cf. Huang [11]. Recent studies by Iyer and Lissenden [12], Casacu and Barlat [13] provide formulations of yield conditions and flow potentials for magnesium alloys and nickel base alloys assuming dependence on the third stress deviator invariant. The simulation of deformation anisotropy was also presented by Casacu and Barlat [13] by modifying the isotropic yield condition. In an earlier paper by Shrivastawa et al. [14], a general form of anisotropic yield condition was discussed with account for the effect of $J_3$.

In Sect. 2 we consider a three-parameter class of isotropic yield conditions depending on $J_2$ and $J_3$ and independent of hydrostatic pressure. The constraints imposed by the convexity condition will be discussed in detail and the parameters will be identified for Ni–Ti shape memory alloys. In Sect. 3 the form of the dissipation function will be derived and the inverse relations will be generated.

## 2 Analysis of three-parameter yield conditions

### *2.1 General formulation*

Consider an isotropic material for which the yield condition can be expressed in terms of the second and third stress deviator invariants $J_2$, $J_3$, namely in the form

$$\mathfrak{F}_1(J_2,J_3) = (J_2)^{3n_1/2} - c\,(J_3)^{n_1} - \tau_{\mathrm{c}}^{3n_1} = 0, \tag{1}$$

where

$$J_2 = \frac{1}{2}s_{ij}s_{ij} = \frac{1}{2}\mathrm{tr}(\boldsymbol{s}^2), \quad J_3 = \frac{1}{3}s_{ik}s_{kl}s_{li} = \frac{1}{3}\mathrm{tr}(\boldsymbol{s}^3) = \det(\boldsymbol{s}), \quad s_{ij} = \sigma_{ij} - \frac{1}{3}\sigma_{kk}\delta_{ij} \tag{2}$$

and $s_{ij}$ denotes the deviatoric part of the Cauchy stress tensor $\sigma_{ij}$, the material parameters are $n_1$, $\tau_c$ and $c$. For $n_1 = 1$ we obtain the yield condition considered by Casacu and Barlat [13], thus

$$\mathfrak{F}_1(J_2,J_3) = (J_2)^{3/2} - c\,J_3 - \tau_{\mathrm{c}}^3 = 0, \tag{3}$$

and for $n_1 = 2$ the condition proposed by Drucker [15],

$$\mathfrak{F}_1(J_2,J_3) = (J_2)^3 - c(J_3)^2 - \tau_{\mathrm{c}}^3 = 0. \tag{4}$$

Let us note that for even exponents $n_1 = 2, 4, 6,\ldots$ the yield condition predicts the same values of the yield stress in tension and compression. However, for odd exponents $n_1 = 1, 3, 5, \ldots$ the yield condition provides different values of the yield stress, thus exhibiting the SD-effect. Introduce the Lode invariants $r$ and $y$,

$$r(\boldsymbol{s}) = [\mathrm{tr}(\boldsymbol{s}^2)]^{1/2} = |\boldsymbol{s}| = \sqrt{2J_2}, \quad y(\boldsymbol{s}) = \cos(3\theta) = \frac{3\sqrt{3}J_3}{2(J_2)^{3/2}} = \sqrt{6}\mathrm{tr}(\boldsymbol{N}^3), \tag{5.1,2}$$

where $r = |\boldsymbol{s}| = (s_{ij}s_{ij})^{1/2}$ and $\theta$ represent the stress radius and its angle with the image of the positive half-axis of principal stress $\sigma_1$ on the octahedral plane, cf. Fig. 2. The Lode invariant $y(\mathbf{s})$ is the homogeneous function of degree zero of the stress deviator. It is bounded, $-1 \le y \le 1$, and

takes the values: $y = 0$ at simple shear ($\theta = 30°$), $y = 1$ at simple tension ($\theta = 0°$) and $y = -1$ at simple compression ($\theta = 60°$). As indicated in Eq. (5.2) it can be expressed in terms of the normalized deviator represented by the unit vector $\boldsymbol{N}$ along the stress radius

$$\boldsymbol{N} = \frac{\boldsymbol{s}}{|\boldsymbol{s}|} = \frac{\boldsymbol{s}}{r}, \quad \mathrm{tr}(\boldsymbol{N}) = 0, \quad \mathrm{tr}(\boldsymbol{N}^2) = 1. \tag{6}$$

In passing we note that this unit tensor has the following mathematical properties:

$$3\det\boldsymbol{N} = \mathrm{tr}(\boldsymbol{N}^3) = \frac{\sqrt{6}}{6}y, \quad \mathrm{tr}(\boldsymbol{N}^4) = \frac{1}{2} \tag{7}$$

which directly follow from the Cayley–Hamilton theorem specified for normalized deviatoric tensors,

$$\boldsymbol{N}^3 = \frac{1}{2}\boldsymbol{N} + \boldsymbol{1}\det\boldsymbol{N} = \frac{1}{2}\boldsymbol{N} + \frac{1}{3}\mathrm{tr}(\boldsymbol{N}^3)\,\boldsymbol{1}. \tag{8}$$

Taking into account Eqs. (5) the yield condition (1) can be transformed as follows:

$$\mathfrak{F}_1(J_2,J_3) = (J_2)^{3n_1/2}\left\{1 - c\left[\frac{J_3}{(J_2)^{3/2}}\right]^{n_1}\right\} - \tau_{\mathrm{c}}^{3n_1} = 0 \;\Leftrightarrow\; \mathfrak{F}_0(J_2,J_3) = rf_0(y) - \sqrt{2}\tau_{\mathrm{c}} = 0, \quad (9.1,2)$$

where

$$f_0(y) = [1 - c_0 y^{n_1}]^{\frac{1}{3n_1}}, \quad c_0 = c\left(\frac{2\sqrt{3}}{9}\right)^{n_1}. \tag{10}$$

Two different yield functions $\mathfrak{F}_1$ (cf. Eq. (1)) and $\mathfrak{F}_0$ (cf. Eq. (9.2)) describe the same yield surface in the $\boldsymbol{s}$-space. The presented transformation illustrates the general mathematical property noted by Hill [16]: the yield function $\mathfrak{F}$ of a star-shaped (with respect to the origin) yield surface can be scaled over the surface so that $(\partial\mathfrak{F}/\partial\sigma_{ij})\sigma_{ij}$ is *uniform*. In the considered case $(\partial\mathfrak{F}_0/\partial s_{ij})s_{ij} = \sqrt{2}\tau_{\mathrm{c}}$ . Since $r$ is the length of the radius-vector in the deviatoric space and $y = \sqrt{6}\mathrm{tr}(\boldsymbol{N}^3)$ (cf. Eqs. (5)), the equation of the yield surface (9.2) in the deviatoric space can also be presented in alternative parametric form

$$\boldsymbol{s} = \frac{\sqrt{2}\tau_{\mathrm{c}}\boldsymbol{N}}{f_0[y(\boldsymbol{N})]},$$

where four independent components of $\boldsymbol{N}$, cf. Eq. (6), play the role of parameters.

More generally, the conical limit surface for pressure sensitive material can be described as follows [17], [18]:

$$\mathfrak{F}(\boldsymbol{\sigma}) \equiv f(y)r(\boldsymbol{s}) + H_1\mathrm{tr}(\boldsymbol{\sigma}) - H_0 = 0, \quad f(y) > 0, \quad f(0) = 1, \tag{11}$$

and its counterpart for pressure-insensitive isotropic metallic solids becomes

$$\mathfrak{F}(\boldsymbol{s}) \equiv f(y)r(\boldsymbol{s}) - \sqrt{2}\tau_{\mathrm{c}} = 0, \quad f(y) > 0, \quad f(0) = 1$$

or

$$\sigma_{\mathrm{ef}}f(y) = \sqrt{3}\tau_{\mathrm{c}}, \tag{12}$$

where $H_0$ and $H_1$ are material parameters, $\sigma_{\mathrm{ef}}$ is the effective Huber–Mises stress, $\sigma_{\mathrm{ef}} = \sqrt{3J_2}$ . The positive-valued function $f(y)$ is called the shape function of the critical state surface. It is scaled here so that $f = 1$ at pure shear. Therefore, for pressure-insensitive materials the constant $\tau_c$ represents the yield (or critical) stress in pure shear. The class of non-singular (regular) yield conditions is defined by scale functions with bounded first derivative $df(y)/dy \equiv f'(y)$. The notion of shape

function was introduced by Podgórski [17], [18] to describe the section of a general conical limit surface made by the deviatoric plane for pressure sensitive materials (concrete, sand and clay). Generalizing the earlier proposals of Lade and Duncan [19], Matsuoka [20] and Ottosen [21] he proposed the trigonometric form of the shape function whose alternative form is

$$f(y) = \frac{1}{\cos(30 - \bar{\beta})} \cos\left[\frac{1}{3}\arccos(\bar{\alpha} y) - \bar{\beta}\right] \tag{13}$$

where $0 \leq \bar{\alpha} < 1$ and $0 \leq \bar{\beta} \leq 30^\circ$ are material parameters.

As remarked in Sect. 1 we shall here analyze simpler exponential and power two-parameter shape functions, and investigate in details the convexity of the described critical surfaces. In calibrating yield conditions with experimental data, an alternative scaling of the shape function may also be convenient. For example, one can write the condition (12) in the equivalent forms

$$\begin{aligned} &\sigma_{\mathrm{ef}} f_1(y) = \sigma_{\mathrm{c}}, \quad f_1(-1) \equiv 1 \;\Leftrightarrow\; r(\boldsymbol{s}) = \frac{\sqrt{2/3}\,\sigma_{\mathrm{c}}}{f_1(y)} \quad \text{or} \\ &\sigma_{\mathrm{ef}} f_2(y) = \sigma_t \quad f_2(1) \equiv 1 \;\Leftrightarrow\; r(\boldsymbol{s}) = \frac{\sqrt{2/3}\,\sigma_t}{f_2(y)}, \end{aligned} \tag{14.1–6}$$

where $\sigma_c$ and $\sigma_t$ denote yield stresses in simple compression and simple tension, respectively. The following connections between these different shape functions occur:

$$f(y) = m f_2(y), \quad f_2(y) = q f_1(y), \quad f(y) = mq f_1(y), \tag{15}$$

where the parameters $m$ and $q$

$$m = \frac{\sqrt{3}\tau_{\mathrm{c}}}{\sigma_t}, \quad q = \frac{\sigma_t}{\sigma_{\mathrm{c}}} \tag{16}$$

specify the tension–compression–shear limit state asymmetry called frequently "the strength differential effect" or SD effect. Let us note that for Huber–Mises yield condition there is $q = m = 1$.

It is shown in Appendix A that the yield surface specified by (12) is *convex* provided the shape function $f(y)$ satisfies the following condition:

$$(1 - y^2) f''(y) - y f'(y) + \frac{f(y)}{9} \geq 0 \tag{17}$$

in the interval $-1 \leq y \leq 1$.

Here and in the subsequent analysis we shall adopt the convention that the superimposed prime denotes the derivative of a function with respect to the argument enclosed in brackets. The convexity condition for differently scaled shape functions is identical to (17), thus $f_1(y)$ or $f_2(y)$ can be substituted into Eq. (17).

### *2.2 Two parameter exponential shape function*

Consider the two-parameters exponential shape function $f_1(y)$ defined by

$$f_1(y) = 1 + b_1\{1 - \exp[-c_1(1 + y)]\} \quad f_1(-1) = 1, \tag{18}$$

where $c_1 \geq 0$ and $b_1$ are constant parameters to be determined from the experimental data. Note that for $c_1 = 0$ or $b_1 = 0$ the condition (18) becomes the Huber–Mises yield criterion.

The convexity condition (17) imposed on the exponential shape function (18) generates the inequality

$$b_1 F_1(y, c_1) \le (1 + b_1), \quad F_1(y, c_1) \equiv 9\left(-c_1^2 y^2 + c_1 y + c_1^2 + \frac{1}{9}\right) e^{[-c_1(y+1)]} \tag{19}$$

which must be satisfied for arbitrary $-1 \le y \le 1$. The careful analysis of the function $F_1(y, c_1)$ leads to the following conclusions:

(i) When $0 \le c_1 \le c_1^* = 8/27$ the function $F_1$ reaches its supremum at the boundary $y = 1$. It is equal to $F_1(1, c_1) = (9c_1 + 1)\exp(-2c_1)$.

(ii) When $c_1 \ge c_1^*$ the function $F_1$ reaches the analytical maximum $F_1\ [y_1(c_1), c_1]$ for

$$y = y_1(c_1) = \frac{1}{2c_1}\left[3 - \sqrt{\frac{49}{9} + 4c_1^2}\right] \tag{20}$$

that belongs to the interval $-1 \le y \le 1$.

(iii) The function $F_1$ reaches its infimum at the boundary $y = -1$ of the interval $-1 \le y \le 1$ . It is equal to $F_1(-1, c_1) = 1 - 9c_1$.

The convexity condition therefore provides the parameter inequalities

$$\beta_2(c_1) \le b_1 \le \beta_1(c_1), \tag{21}$$

where

$$\begin{aligned} \beta_1(c_1) &= \begin{cases} \frac{1}{F_1(1,c_1)-1} & \text{for } c_1 \le c_1^* = 8/27 \\ \frac{1}{F_1[y_1(c_1),c_1]-1} & \text{for } c_1 > c_1^* = 8/27, \end{cases} \\ \beta_2(c_1) &= \frac{1}{F_1(-1, c_1) - 1} = \frac{-1}{9c_1}. \end{aligned} \tag{22}$$

The graphical illustration of the convexity inequalities (21) is presented in Fig. 1a. It is seen in Fig. 1a that for increasing values of parameter $c_1$ the convexity interval of the variation of $b_1$ becomes narrow with $b_1 \to 0$ for large $c_1$. Determining from Eqs. (14.1) and (18) the asymmetry parameters $m$ and $q$, cf. Eqs. (16), we have

$$f_1(1) = 1 + b_1(1 - e^{-2c_1}) = q^{-1}, \quad f_1(0) = 1 + b_1(1 - e^{-c_1}) = (qm)^{-1} \tag{23}$$

and

$$c_1 = \ln\left(\frac{1 - qm}{m - 1}\right), \quad b_1 = \frac{(1 - qm)^2}{qm[2 - m(1 + q)]} \tag{24}$$

provided that either ($m > 1$ and $qm < 1$) or ($m < 1$ and $qm > 1$) holds.

Two bounding curves of Fig. 1a can now be mapped onto the bounding curves in the $m - c_1$ and $q - c_1$ planes shown in Fig. 1b. Their equations are ($i = 1, 2$)

$$\begin{aligned} q &= q_i(c_1) = [1 + \beta_i(c_1)(1 - e^{-2c_1})]^{-1}, \\ m &= m_i(c_1) = [1 + \beta_i(c_1)(1 - e^{-2c_1})][1 + \beta_i(c_1)(1 - e^{-c_1})]^{-1}, \end{aligned} \tag{25}$$

where $\beta_1(c_1)$ and $\beta_2(c_1)$ are defined by Eqs. (22). The convexity domain ($q_1 \le q \le q_2$, $m_2 \le m \le m_1$) shown in Fig. 1b specifies the variation of the asymmetry parameters $q$, $m$ satisfying inequalities (21). Figure 1c presents the forms of the exponential shape functions for selected parameters corresponding to the border of the convexity region (cf. Eqs. (22)). When $q = [1/f_1(1)] < 1$ the functions $f_1(y)$ are increasing, when $q > 1$ they are decreasing functions of the Lode parameter $y$.

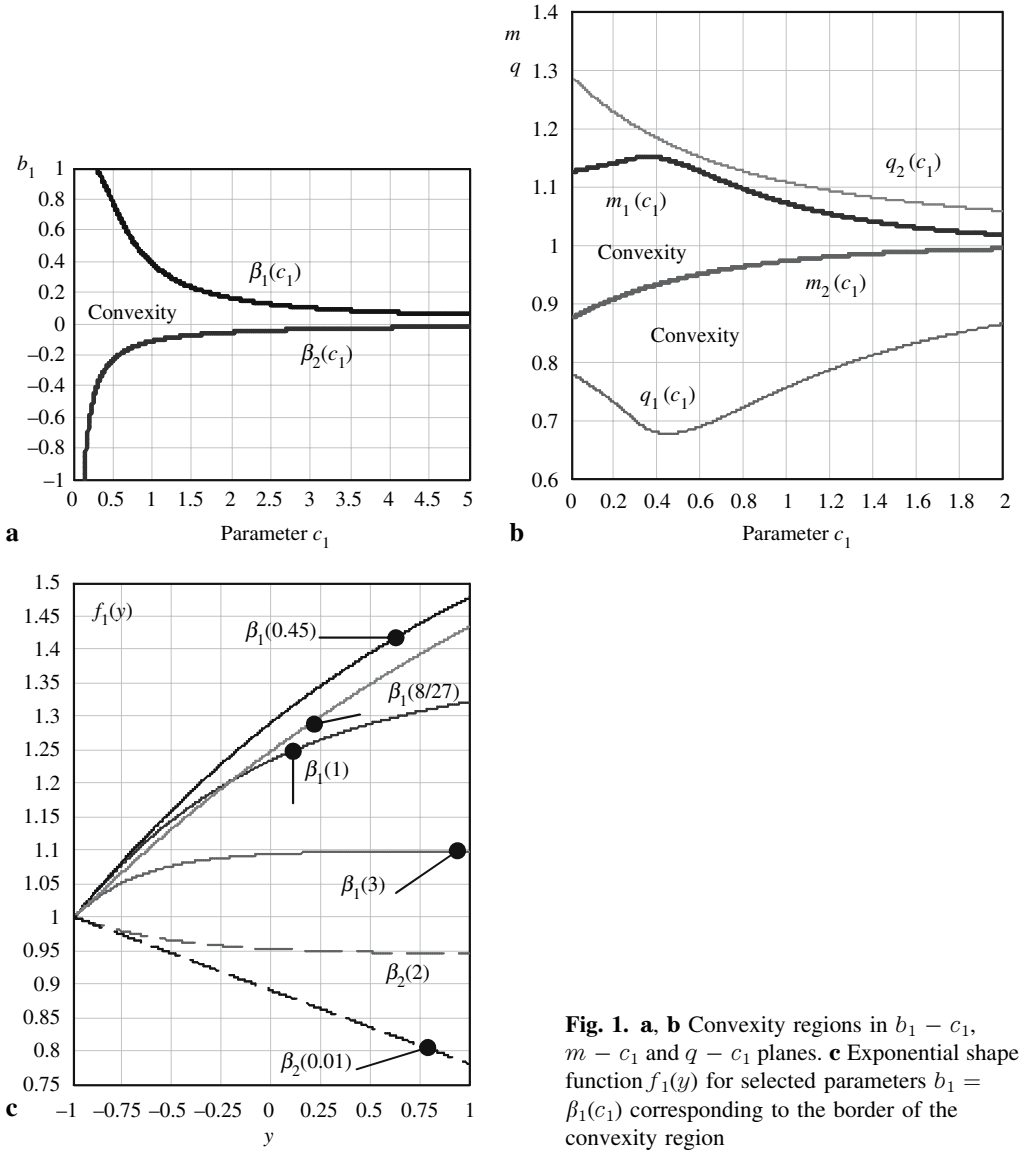


**Fig. 1. a**, **b** Convexity regions in $b_1 - c_1$, $m - c_1$ and $q - c_1$ planes. **c** Exponential shape function $f_1(y)$ for selected parameters $b_1 = \beta_1(c_1)$ corresponding to the border of the convexity region

Introduce the non-dimensional effective stress $r_1$ defined as follows:

$$r_1 \equiv \frac{\sigma_{\text{ef}}}{\sigma_{\text{c}}} = \frac{\sqrt{3/2}r(\boldsymbol{\sigma})}{\sigma_{\text{c}}} = \frac{1}{f_1(\cos 3\theta)}. \tag{26}$$

The geometrical loci of the relation (26) for the exponential shape function on the octahedral plane are presented in Fig. 2a, b for selected parameters corresponding to the border of the convexity region.

The thermodynamics of pseudoelasticity in shape memory alloys developed by Raniecki and Lexcellent [9] employs the notion of the shape function to describe the pseudoelasticity limits, i.e. the limit stability states of austenite where the austenite–martensite phase transitions are initiated. The exponential form of the shape function was applied in Raniecki et al. [22] to describe the limits

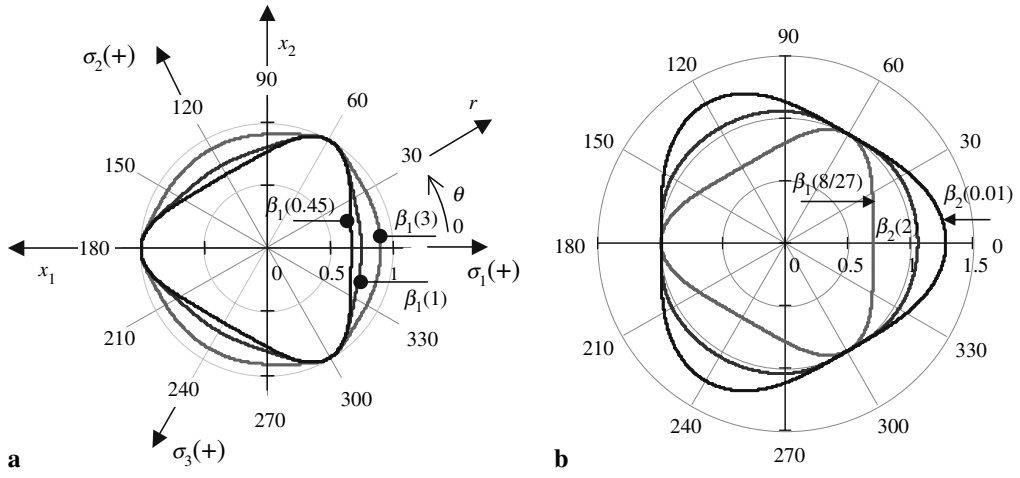


**Fig. 2.** Examples of exponential yield loci: **a** for the case $q<1$ and the values of $c_1 = 0.45, 1.0, 3.0$; **b** for the cases $q<1$, $c_1 = 8/27$ and $q > 1$, $c_1 = 0.01$, $c_1 = 2.0$

in Ti-51 at %Ni shape memory alloy. The proportional torsion–compression–tension tests were performed at $y = 0, \pm 1, \pm 11/16$ under controlled stresses at temperatures $T = 316$ K and $T = 322.5$ K. The specified parameter values are $b_1 = 0.463$ and $c_1 = 0.777$. The continuous line in Fig. 3a presents the exponential shape function for this alloy. The experimental points are marked by squares and crosses. The image of the surface on the octahedral plane for the temperature $T = 322.5$ K is shown in Fig. 3b. Squares denote the experimental critical stresses (offset $0.2\%$) presented by Raniecki et al. [22]. It is seen that the proposed condition closely simulates the experimental data. The theoretical (corresponding to the specified parameters) limit locus in the principal stress plane is presented in Fig. 3c for the situation when $\sigma_3 = 0$. The symbol $\sigma_c$ occurring in this figure denotes the critical stress in simple compression. It is equal to $604$ MPa for the investigated TiNi alloy.

Lexcellent et al. [10] used the trigonometric form of shape function

$$f_2(y) = \cos\left\{\frac{1}{3}\arccos[1 - a_2(1-y)]\right\}$$

and found that the results of their experiments on CuZnAl and CuAlBe alloys are well fitted when $a_2 = 0.7$. With accuracy lesser than $1\%$ their theoretical shape function curve can equivalently be described by the exponential shape function (18) with $b_1 = 0.4$ and $c_1 = 0.52$. It is shown by the dotted line in Fig. 3a. It is seen that CuZnAl and CuAlBe alloys exhibit less pronounced SD effect than TiNi alloy.

### *2.3 Two-parameter power shape function*

The alternative, relatively simple critical condition can be specified by a two-parameter power shape function of the type (12)

$$f(y) = (1 + by)^n, \quad f(0) = 1, \tag{27}$$

where

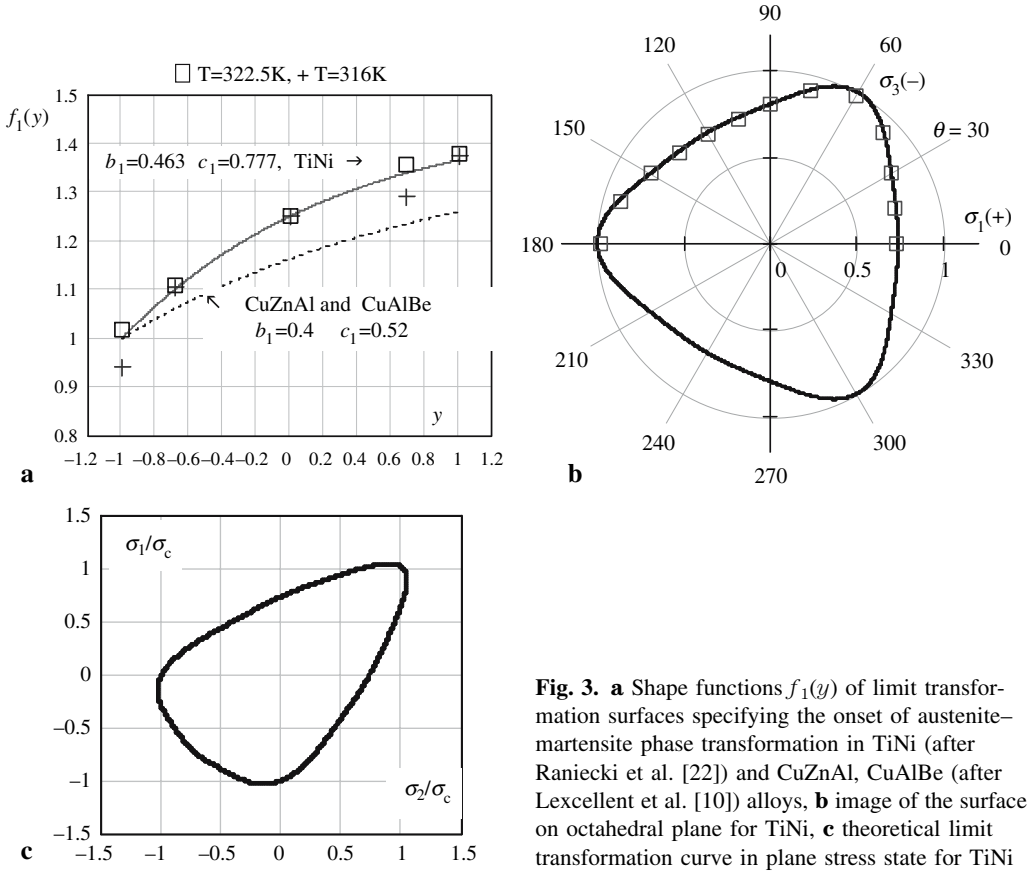


**Fig. 3.** **a** Shape functions $f_1(y)$ of limit transformation surfaces specifying the onset of austenite–martensite phase transformation in TiNi (after Raniecki et al. [22]) and CuZnAl, CuAlBe (after Lexcellent et al. [10]) alloys, **b** image of the surface on octahedral plane for TiNi, **c** theoretical limit transformation curve in plane stress state for TiNi

$$|b| \leq 1 \tag{28}$$

and $n$ is an arbitrary exponent. For $n = 1/3$ the combination of Eqs. (27) and (12) reduces to Casacu's and Barlat's [13] condition. The shape function in the form (27) for $n = -1$ ($b < 0$) was employed by Millis and Zimmerman [23] as the failure condition for concrete, whereas for dry sand Gudehus [24] proposed the function (27) for $n = -1/2$, ($b < 0$).

The convexity condition (17) now takes the form

$$F_2(y, b, n) \equiv A_0 y^2 + B_0 y + C_0 \geq 0, \tag{29}$$

where

$$A_0 = b^2(1 - 9n^2), \quad B_0 = b(2 - 9n_1), \quad C_0 = 1 + 9b^2 n(n-1). \tag{30}$$

By analyzing the set of inequalities (28) and (29) we arrive at the following conclusions:

(i) When $|n| \geq 1/3$ implying $A_0 \leq 0$, the necessary and sufficient condition for (28) and (29) to hold is

$$b^2 \leq \frac{1}{(1 - 9n)^2}. \tag{31}$$

This case corresponds to the situation when the smaller root of the equation $F_2 = 0$ is less or equal to $-1$ and the greater root is larger or equal to 1.

(ii) When $-1/3 \le n \le 0$ or $n^* \equiv 3/11 \le n \le 1/3$ implying $A_0 \ge 0$, the inequality (31) is also necessary and sufficient for the set of inequalities (28) and (29) to occur. This result corresponds to the situation when either the smaller root of $F_2 = 0$ is greater than 1 or the larger root is smaller than $-1$.

(iii) When $0 \le n \le n^* = 3/11$ the non-positive discriminant of $F_2 = 0$ determines the necessary and sufficient condition for (28) and (29) to hold, which implies

$$|b| \le b_0(n) = \sqrt{\frac{12 - 39n}{12(1-n)(1-9n^2)}}. \tag{32}$$

Hence, the convexity condition of the yield surface (12) with the power shape function (27) can be expressed as follows:

$$|b| \le \alpha(n), \tag{33}$$

where

$$\alpha(n) = \begin{cases} \dfrac{1}{1-9n} & \text{if } n \le 0 \\ \dfrac{1}{9n-1} & \text{if } n \ge n^* = \dfrac{3}{11} \\ b_0(n) & \text{otherwise.} \end{cases} \tag{34}$$

The graphical image of the condition (34) in the $(b,n)$-plane is shown in Fig. 4a. For the illustration purpose the points B and D corresponding to $n = n^* = 3/11$ are marked. It is seen that the convexity domain is narrowing for increasing or decreasing values of $n$ from zero value.

From Eq. (27) it follows that

$$f(1) = m = (1+b)^n, \quad f(-1) = mq = (1-b)^n, \tag{35}$$

and the boundaries of the convexity region can be presented in the $(m, n)$ and $(q, n)$ planes. The parametric forms of the convexity boundaries $b = \alpha(n)$ and $b = -\alpha(n)$ are

$$q = q_1(n) = \frac{[1-\alpha(n)]^n}{[1+\alpha(n)]^n}, \quad m = m_1(n) = [1+\alpha(n)]^n \tag{36}$$

and

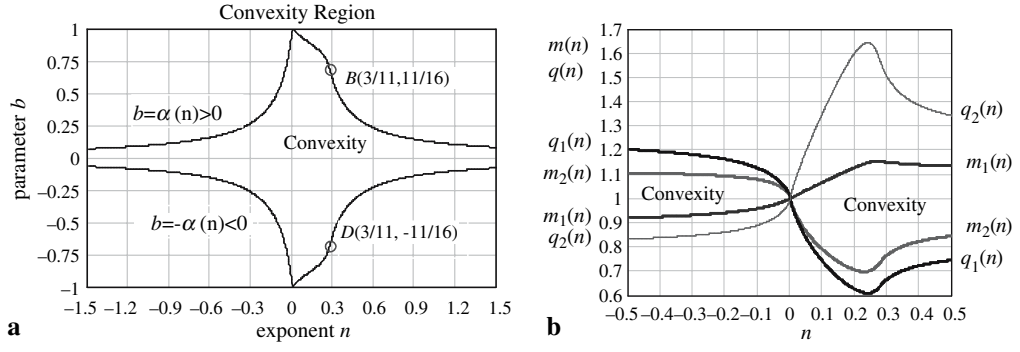


**Fig. 4.** The power shape function of the yield surface: **a** convexity domain in the $(b, n)$-plane, **b** convexity domains in $(m, n)$ and $(q, n)$ planes

$$q = q_2(n) = \frac{[1+\alpha(n)]^n}{[1-\alpha(n)]^n}, \quad m = m_2(n) = [1-\alpha(n)]^n, \tag{37}$$

where the function $\alpha(n)$ is defined by (34). The convexity domain boundaries in the ($m$, $n$) and ($q$, $n$) planes are shown in Fig. 4b. Let us note that for $n = 1/3$ [or $n_1 = 1$ for the exponent occurring in the yield condition (1)] the presented specification of the convexity domain $|b| \leq 1/2$ (or equivalently $|c| \leq 3\sqrt{3}/4$ , cf. Eq. (1)) does not agree with the result ($|c| \leq 3\sqrt{3}/2$) obtained by Casacu and Barlet [13].

By comparison of the plots presented in Figs. 1b and 4b it is seen that the convex power yield function (27) is capable to describe higher strength asymmetry than the exponential function (19). For instance, in the convex region the minimum values of the asymmetry parameter $q$ are $q_{\min} \simeq 0.609$ (for $n \simeq 0.24$, $m \simeq 1.148$, $b \simeq 0.775$) and $q_{\min} \simeq 0.676$ (for $m \simeq 1.144$, $b_1 \simeq 0.807$, $c_1 \simeq 0.45$) when power and exponential shape functions are applied, respectively. Likewise, in the convex region the maximum values of the parameter $q$ are $q_{\max} \simeq 1.642$ (for $n \simeq 0.24$, $m \simeq 0.7$, $b \simeq -0.775$) for the power shape function and $q_{\max} \simeq 1.282$ (for $m \simeq 0.877$, $c_1 = 0.01$ $b_1 \simeq -11.1$) for the exponential shape function.

The examples of the power shape functions at the boundary of the convexity domain setting $b = \alpha(n)$ and $b = -\alpha(n)$ are presented in Fig. 5

Figure 6a, b presents the loci of the yield condition (12) for the power shape function (27) on the octahedral plane for selected parameters at the border of the convexity region.

## 3 Rigid-plastic solids: flow rule and dissipation function

### *3.1 Inverse relations*

In this Section we shall discuss the flow rule and inverse relations between stress and strain rate tensors generated by the dissipation function which is a dual potential to the yield condition for a rigid-plastic response. Denote by $\boldsymbol{D}$ the Eulerian strain rate which for a pressure-insensitive material and the associated flow rule is the deviatoric tensor. The flow rule associated with the yield condition (12) takes the form

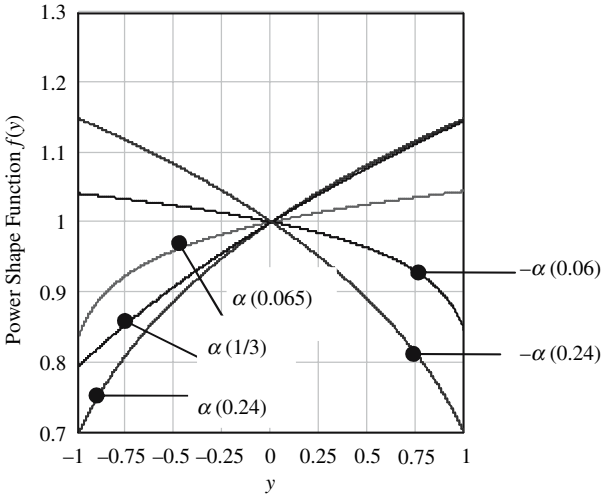


**Fig. 5.** Power shape functions at the boundary of the convexity domain

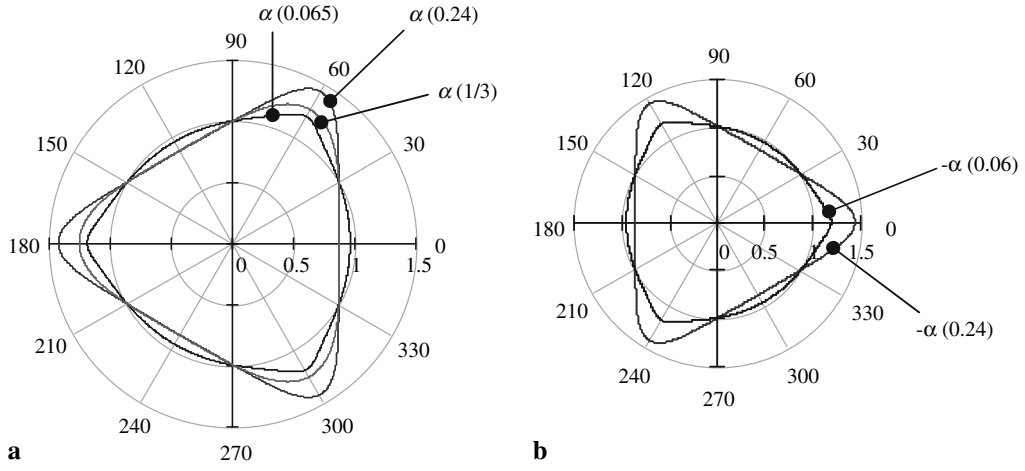


**Fig. 6.** Examples of yield loci for the power shape function at the border of the convexity domain: **a** for the asymmetry parameter $q < 1$, **b** for $q > 1$

$$\boldsymbol{D} = r_\varepsilon(\boldsymbol{D})\boldsymbol{n}(\boldsymbol{s}), \tag{38}$$

where

$$r_\varepsilon(\boldsymbol{D}) = |\boldsymbol{D}| = \sqrt{\mathrm{tr}(\boldsymbol{D}^2)}, \quad \boldsymbol{n}(\boldsymbol{s}) = \frac{\partial\tilde{\mathfrak{F}}/\partial\boldsymbol{s}}{|\partial\tilde{\mathfrak{F}}/\partial\boldsymbol{s}|} = \frac{\boldsymbol{D}}{|\boldsymbol{D}|} \tag{39}$$

and $\boldsymbol{n}(\boldsymbol{s})$ is the unit normal tensor to the yield surface.

To determine the inverse relation we shall introduce the orthonormal reference frame $\boldsymbol{n},\ \boldsymbol{n}^\perp$ in the strain-rate deviator space and the conjugate frame $\boldsymbol{N},\ \boldsymbol{N}^\perp$ in the stress deviator space specified by the normalized tensors (Fig. 7). Let us note that

$$\frac{\partial r(\boldsymbol{s})}{\partial\boldsymbol{s}} = \boldsymbol{N}, \quad r\frac{\partial y}{\partial\boldsymbol{s}} = 3\sqrt{1-y^2}\boldsymbol{N}^\perp(\boldsymbol{s}), \tag{40}$$

where $\boldsymbol{N}^\perp$ is the normalized tensor orthogonal to $\boldsymbol{N}$, so that

$$\boldsymbol{N}^\perp(\boldsymbol{s}) \equiv \frac{1}{\sqrt{1-y^2}}\left[\sqrt{6}(\boldsymbol{N}^2 - \frac{1}{3}\boldsymbol{1}) - y\boldsymbol{N}\right], \quad \mathrm{tr}[(\boldsymbol{N}^\perp)^2] = 1, \quad \mathrm{tr}(\boldsymbol{N}^\perp) = 0, \ \ (\boldsymbol{1})_{ij} = \delta_{ij}, \tag{41.1–4}$$

and moreover $\boldsymbol{N}$ and $\boldsymbol{N}^\perp$ satisfy the orthogonality condition, thus

$$\mathrm{tr}(\boldsymbol{N}\boldsymbol{N}^\perp) = 0 \tag{42}$$

and

$$\partial[rf(y)]/\partial\boldsymbol{s} = \partial\tilde{\mathfrak{F}}/\partial\boldsymbol{s} = f\boldsymbol{N} + 3f'(y)\sqrt{1-y^2}\boldsymbol{N}^\perp. \tag{43}$$

The normalized deviatoric tensor $\boldsymbol{n}(\boldsymbol{s})$ $(\mathrm{tr}(\boldsymbol{n}^2) = 1)$ normal to the yield surface (12) can be decomposed along $\boldsymbol{N}$ and $\boldsymbol{N}^\perp$ as follows:

$$\boldsymbol{n}(\boldsymbol{s}) = A\boldsymbol{N} + B\boldsymbol{N}^\perp, \tag{44}$$

where

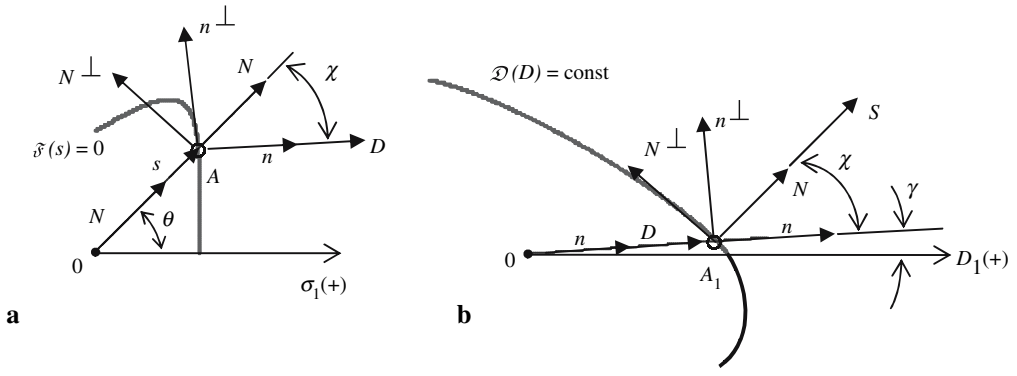


**Fig. 7.** Reference frames $\boldsymbol{n}$, $\boldsymbol{n}^{\perp}$ and $\boldsymbol{N}$, $\boldsymbol{N}^{\perp}$ in **a** stress deviator space and **b** strain rate deviator space

$$
\begin{aligned}
&A(y) = \left\{1 + 9(1-y^2)\left[\frac{f'(y)}{f(y)}\right]^2\right\}^{-1/2} = \mathrm{tr}(\boldsymbol{N}\boldsymbol{n}) = \cos(\chi),\\
&B(y) = 3\frac{f'(y)}{f(y)}\sqrt{1-y^2}\cos(\chi) = \mathrm{tr}(\boldsymbol{n}\boldsymbol{N}^{\perp}) = j^*\sin(\chi),\\
&A^2 + B^2 = 1, \quad j^* = \mathrm{sign}[f'(y)],
\end{aligned}
\tag{45.1–4}
$$

and $\chi$ is the angle between the direction of strain rate and stress in the deviatoric space, cf. Fig. 7. Thus, the normalized strain rate tensor $\boldsymbol{n}$ can be specified from Eqs. (44) and (45).

In order to derive the inverse relations specifying the stress deviator in terms of the strain rate deviator, it is assumed that $\boldsymbol{n}$ is prescribed and $\boldsymbol{N}$ is to be determined.

Let us first define the normalized stress deviator $\boldsymbol{n}^{\perp}$ orthogonal to $\boldsymbol{n}$, thus

$$
\boldsymbol{n}^{\perp} \equiv -B\boldsymbol{N} + A\boldsymbol{N}^{\perp}, \quad \mathrm{tr}(\boldsymbol{n}\boldsymbol{n}^{\perp}) = 0, \quad \mathrm{tr}(\boldsymbol{n}^2) = 1, \quad \mathrm{tr}(\boldsymbol{n}) = 0, \tag{46.1–4}
$$

and in view of (44) and (46) we can write

$$
\boldsymbol{N} = A\boldsymbol{n} - B\boldsymbol{n}^{\perp}, \quad \boldsymbol{N}^{\perp} = B\boldsymbol{n} + A\boldsymbol{n}^{\perp}. \tag{47}
$$

Considering the octahedral strain rate plane, Fig. 7, introduce the Lode parameter $x(\boldsymbol{D})$ specified by the angle $\gamma$ between strain rate vector and the image of principal strain rate axis $D_1$, thus

$$
x(\boldsymbol{D}) = \frac{3\sqrt{3}I_3}{2(I_2)^{3/2}} = \sqrt{6}tr[\boldsymbol{n}^3(\boldsymbol{D})] = \cos(3\gamma), \tag{48}
$$

where

$$
2I_2 = r_{\varepsilon}^2(\boldsymbol{D}), \quad r_{\varepsilon} \equiv \sqrt{\mathrm{tr}(\boldsymbol{D}^2)}, \quad I_3 = \det(\boldsymbol{D}) = \mathrm{tr}[(\boldsymbol{D})^3]/3 \tag{49}
$$

and $I_1 = 0$, $I_2$, $I_3$ are the basic invariants of $\boldsymbol{D}$. Referring to Appendix B, the relation between the parameters $x$ and $y$ can be exposed in two alternative forms:

$$
x = x(y) = \sqrt{6}\,\mathrm{tr}(\boldsymbol{n}^3) = y(A^3 - 3AB^2) + \sqrt{1-y^2}(3A^2B - B^3) = \cos[3(\theta - j^*\chi)] \tag{50}
$$

or

$$
x = x(y) = \cos\{\arccos(y) - 3j^*\arccos[A(y)]\} \;\Rightarrow\; \theta = \gamma + j^*\chi, \tag{51.1,2}
$$

where $j^* = \text{sign}[f'(y)]$. Here, $A(y)$ and $B(y)$ are specified by (45), since $A(\pm 1) = 1$ and $B(\pm 1) = 0$ it follows from Eq. (50) that $x(\pm 1) = \pm 1$. The other mathematical property of the representations (50) and (51) is discussed in Appendix B. Define the function $g(x)$

$$g(x) \equiv \frac{\cos[\chi(x)]}{f[y(x)]} = \left[\frac{A(y)}{f(y)}\right]_{y=y(x)}, \tag{52}$$

where $y(x)$ is the inverse of $x(y)$ specified by Eq. (50). The following differential relation between $f(y)$ and $g(x)$ holds:

$$\sqrt{1-y^2}\frac{f'(y)}{f(y)} + \sqrt{1-x^2}\frac{g'(x)}{g(x)} = 0. \tag{53}$$

Therefore, the dual form of Eq. (45) becomes

$$\begin{aligned} A(x) &= A[y(x)] = \left\{1 + 9(1-x^2)\left[\frac{g'(x)}{g(x)}\right]^2\right\}^{-1/2} = \text{tr}(\boldsymbol{N}\boldsymbol{n}) = \cos[\chi(x)], \\ B(x) &= B[y(x)] = -3\frac{g'(x)}{g(x)}\sqrt{1-x^2}\cos(\chi) = \text{tr}(\boldsymbol{n}\boldsymbol{N}^{\perp}) = j^*\sin[\chi(x)], \\ A^2 &+ B^2 = 1, \quad j^* = \text{sign}[f'(y)] = -\text{sign}[g'(x)]. \end{aligned} \tag{54.1–4}$$

If the dual function $g(x)$ is known then the function $\chi(x)$ is determined from (54.1), and the inverse relation $y(x)$ directly follows from Eq. (51), thus

$$y = y(x) = \cos\{\arccos(x) + 3j^*\arccos[A(x)]\} \tag{55}$$

or

$$y = y(x) = \sqrt{6}\,\text{tr}(\boldsymbol{N}^3) = x(A^3 - 3AB^2) - \sqrt{1-x^2}(3A^2B - B^3) = \cos[3(\gamma + j^*\chi)], \tag{56}$$

where

$$\theta = \gamma + j^*\chi, \quad j^* = -\text{sign}[g'(x)].$$

Referring to Appendix B the relation between $\boldsymbol{n}^{\perp}$ and $\boldsymbol{n}$ is of the form

$$\boldsymbol{n}^{\perp}(\boldsymbol{D}) \equiv \frac{1}{\sqrt{1-x^2}}\left[\sqrt{6}(\boldsymbol{n}^2 - \frac{1}{3}\boldsymbol{1}) - x\boldsymbol{n}\right], \quad \text{tr}(\boldsymbol{n}^{\perp}) = 0, \quad \text{tr}(\boldsymbol{n}^{\perp})^2 = 1, \tag{57.1–3}$$

which is the same as the relation between $\boldsymbol{N}$ and $\boldsymbol{N}^{\perp}$ , cf. Eq. (41.1). Both relations are independent of the selected scale function $f(y)$.

For the exponential shape function defined by Eq. (18) we have $j^* = \text{sign}(b_1)$ ($j^* = 0$ for $b_1 = 0$) and

$$A(y) = \cos(\chi) = [1 + \tan^2(\chi)]^{-1/2}, \quad \tan^2(\chi) = \frac{9(1-y^2)b_1^2c_1^2e^{-2c_1(1+y)}}{[1 + b_1(1 - e^{-c_1(1+y)})]^2}. \tag{58}$$

The plot of the relation between the $x$ and $y$ parameters for selected values of the constants $\beta_1(c_1)$ and $\beta_2(c_1)$, at the border of the convexity domain, cf. Eq. (22), is shown in Fig. 8

For the power shape function defined by Eq. (27) we have $j^* = \text{sign}(bn)$, $j^* = 0$ for $b = 0$ or $n = 0$, and

$$\tan^2(\chi) = 9b^2n^2\frac{1-y^2}{(1+by)^2}, \tag{59}$$

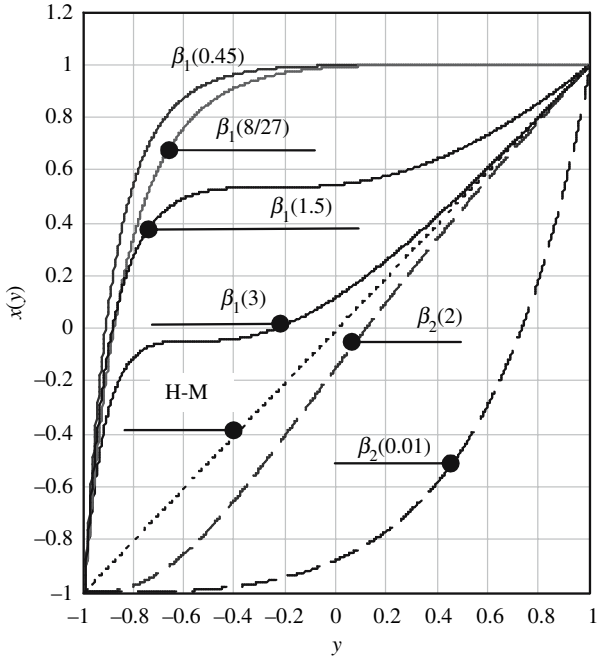


**Fig. 8.** Relations between invariants $x(\boldsymbol{D}) = \sqrt{6}\,\mathrm{tr}(\boldsymbol{n}^3)$ and $y(\boldsymbol{s}) = \sqrt{6}\,\mathrm{tr}(\boldsymbol{N}^3)$ for selected parameters of exponential yield surfaces

The relations $x(y)$ for selected parameters at the border of the convexity region specified by Eq. (29) are shown in Fig. 9. The diagonal dotted straight line presented in Figs. 8 and 9 represents the $x(y)$ relation for the Huber–Mises yield condition.

### *3.2 The dissipation function*

For rigid-plastic solids the dissipation power per unit of volume associated with the yield condition (12) can be expressed as follows:

$$\mathfrak{D} \equiv \mathrm{tr}(\boldsymbol{s}\boldsymbol{D}) = r(\boldsymbol{s}) r_\varepsilon(\boldsymbol{D}) \mathrm{tr}(\boldsymbol{N}\boldsymbol{n}) = r(\boldsymbol{s}) r_\varepsilon(\boldsymbol{D}) \cos(\chi) = \sqrt{2}\tau_c r_\varepsilon(\boldsymbol{D}) \frac{\cos(\chi)}{f(y)}. \tag{60}$$

Introducing the inverse function $g(x)$ defined by (52), we can also define the dissipation function $\mathfrak{D}(\boldsymbol{D})$ of strain rate as

$$\mathfrak{D}(\boldsymbol{D}) \equiv \sqrt{2}\tau_c r_\varepsilon(\boldsymbol{D}) g(x). \tag{61}$$

Since by direct differentiation of Eq. (49) we have

$$\frac{\partial r_\varepsilon(\boldsymbol{D})}{\partial \boldsymbol{D}} = \boldsymbol{n}, \quad r_\varepsilon \frac{\partial x}{\partial \boldsymbol{D}} = 3\sqrt{1-x^2}\,\boldsymbol{n}^\perp(\boldsymbol{D}), \tag{62}$$

where $\boldsymbol{n}^\perp(\boldsymbol{D})$ is given by Eq. (57), the following expression for the gradient of the dissipation function can be derived in view of Eqs. (52) and (54), thus

$$\frac{\partial[\mathfrak{D}(\boldsymbol{D})]}{\partial \boldsymbol{D}} = \sqrt{2}\tau_c g \left[\boldsymbol{n} + 3\sqrt{1-x^2}\left(\frac{g'(x)}{g(x)}\right)\boldsymbol{n}^\perp(\boldsymbol{D})\right] = r[A(x)\boldsymbol{n} - B(x)\boldsymbol{n}^\perp]. \tag{63}$$

As the dissipation function is homogeneous of degree one with respect to strain rate and generates stress by the potential rule, we have

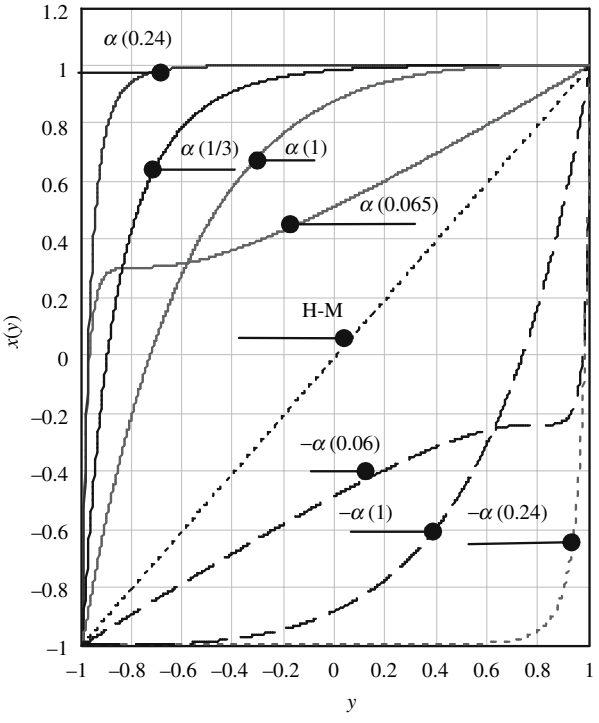


**Fig. 9.** Relations between invariants $x(\boldsymbol{D}) = \sqrt{6}\,\mathrm{tr}(\boldsymbol{n}^3)$ and $y(\boldsymbol{s}) = \sqrt{6}\,\mathrm{tr}(\boldsymbol{N}^3)$ for selected parameters of power yield functions

$$\boldsymbol{s} = \frac{\partial \mathfrak{D}(\boldsymbol{D})}{\partial \boldsymbol{D}}, \quad r(\boldsymbol{s}) = |\partial \mathfrak{D}/\partial \boldsymbol{D}|, \quad \boldsymbol{N} = \frac{1}{r(\boldsymbol{s})}\,\frac{\partial \mathfrak{D}(\boldsymbol{D})}{\partial \boldsymbol{D}}, \tag{64}$$

and the gradient expressions (63) provide the stress–strain rate relations. It follows from Eq. (61) that $g(x)$ plays the role of a shape function of the surface of constant dissipation rate, $\mathfrak{D} = \mathrm{const}$ , in the strain-rate space. It is defined by Eq. (52) in terms of the yield surface shape function $f(y)$ scaled so that $f(0) = 1$. When other scales of the yield shape function (cf. Eq. (14)) are used to define the shape function of constant dissipation rate, e.g.,

$$g_1(x) = \frac{\cos[\chi(x)]}{f_1[y(x)]}, \quad g_2(x) = \frac{\cos[\chi(x)]}{f_2[y(x)]}, \tag{65}$$

we have in view of Eq. (14)

$$g_1(x) = qmg(x), \quad g_2(x) = mg(x), \quad g_1(-1) = 1, \quad g_2(1) = 1 \tag{66}$$

and

$$\frac{\mathfrak{D}(\boldsymbol{D})}{r_\varepsilon(\boldsymbol{D})} = \sqrt{2}\tau_c g(x) = \sqrt{\frac{2}{3}}\sigma_c g_1(x) = \sqrt{\frac{2}{3}}\sigma_t g_2(x). \tag{67}$$

Illustrative plots of $g_1(x)$ dual to exponential yield shape functions are presented in Fig. 10 for the selected parameters corresponding to the border of the convexity domain.

Define the dimensionless equivalent strain rate by

$$R_{1\varepsilon} \equiv \frac{\sqrt{2/3}\sigma_c}{\mathfrak{D}}\, r_\varepsilon(\boldsymbol{D}) \tag{68}$$

and the corresponding function $R_{1\varepsilon}(\gamma)$ following from (68) by

$$R_{1\varepsilon}(\gamma) = \frac{1}{g_1[\cos(3\gamma)]}. \tag{69}$$

The dual potentials are presented in the octahedral plane in Fig. 11. To illustrate the duality, two points A and $A_1$ are marked on the potential loci. The point $A_1$ is the dual image of A in the mapping (64). The normal to the yield locus at A has the direction $0{-}A_1$, whereas the normal to the dissipation potential locus (69) at $A_1$ is represented by the line 0–A.

The shape functions $g_1(x)$ of the constant dissipation potential dual to the power shape functions $f(y)$ are plotted in Fig. 12 for the selected values of parameters corresponding to the border of the convexity region.

It is seen that the curvatures of curves plotted in Fig. 12 for $n > 0$ and $b = \alpha(n) > 0$ are relatively small, therefore it may be convenient to employ the approximate linear function, thus

$$g_1^A(x) \equiv 1 - \frac{1}{2}\left[1 - \left(\frac{1-b}{1+b}\right)^n\right](x+1) \tag{70}$$

for which the dissipation function is expressed as follows:

$$\mathfrak{D}^A(\boldsymbol{D}) \equiv \sqrt{2/3}\sigma_c r_\varepsilon(\boldsymbol{D}) g_1^A[x(\boldsymbol{D})] = \sqrt{2/3} r_\varepsilon(\tilde{\sigma} - 0.5\,[\![\sigma]\!]x) \quad \tilde{\sigma} = 0.5(\sigma_c + \sigma_t), \quad [\![\sigma]\!] = \sigma_c - \sigma_t. \tag{71}$$

The relative error $\Delta_D \equiv (g_1 - g_1^A)/g_1$ associated with this approximation is presented in Fig. 13. For $n \geq 1/3$ it is less than 8%.

The illustrative comparison of geometrical images of the power yield condition and the associated constant dissipation rate functions condition is shown in Fig. 14. Two dual points A and $A_1$ are also marked in this figure. In this case the yield curves are not tangent at rounded corners to the constant dissipation rate loci because the functions $f(y)$ and $g_1(x)$ have different scales: $f(0) = 1$, $g_1(-1) = 1$, $g_1(0) \neq 1$, $f(-1) \neq 1$.

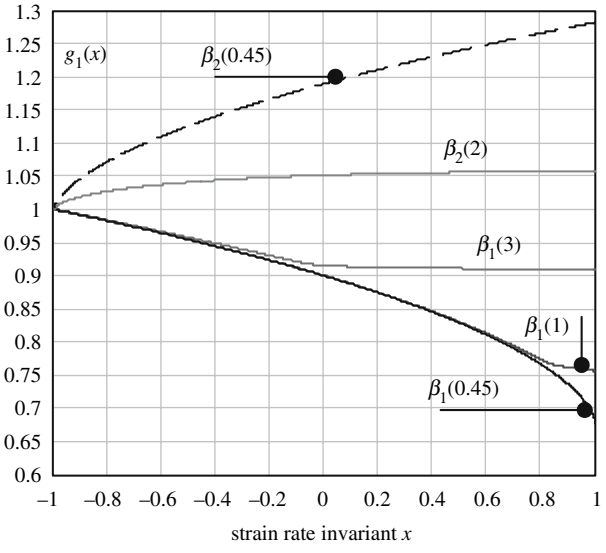


**Fig. 10.** Shape functions $g_1(x)$ of constant dissipation potential surface associated with the dual exponential yield surfaces for selected parameters at the border of the convexity domain

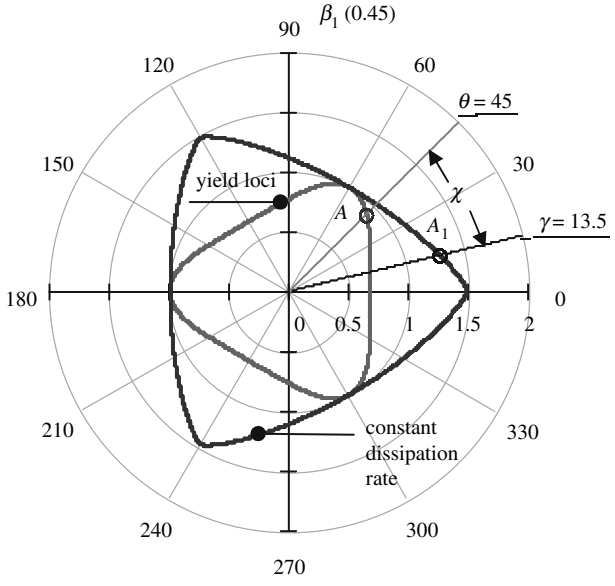


**Fig. 11.** Loci of dual potentials associated with the exponential yield functions in the $\pi$-plane. Parameter values are $q_{\min} \simeq 0.676$, $c_1 = 0.45$, $b_1 = \beta_1(0.45) = 0.807$

## 4 Concluding remarks

The present paper provides the analysis of three-parameter yield conditions for hydrostatic stress independent material response, but affected by the third stress deviator invariant. The SD effect associated with different yield stresses in tension and compression can naturally be accounted for. There are numerous classes of modern materials exhibiting SD effect, and their plastic response could be specified by applying the present condition. It turns out that the convexity condition sets an essential constraint on the range of variation of material parameters for both exponential and power shape function. The dual potential corresponding to the dissipation rate function was also specified. The aim of this paper is to provide a theoretical framework of constitutive relations for modern materials. The identification of material parameters can then be carried out for specific cases of tested materials. The account for the mixed isotropic and kinematic hardening can be introduced by applying the proposed forms of yield conditions and dissipation functions.

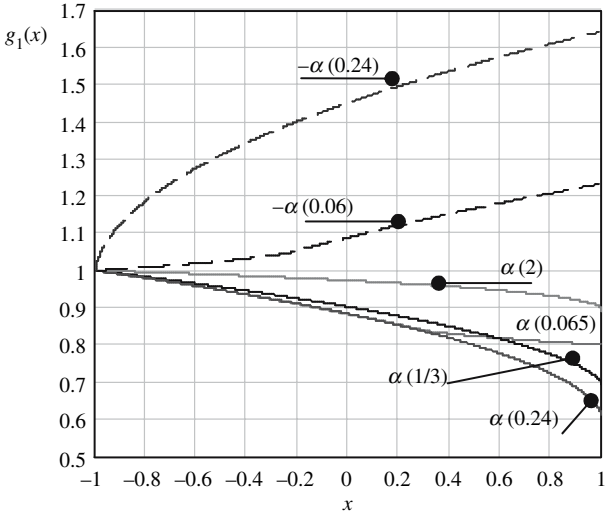


**Fig. 12.** Shape functions $g_1(x)$ of the surface of constant dissipation potentials associated with the dual power yield surfaces for selected parameters at the border of the convexity region

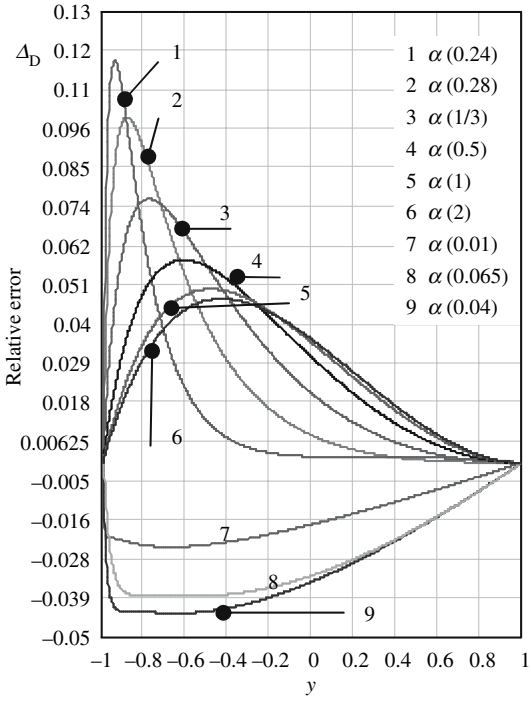


**Fig. 13.** Relative error associated with the linear approximation of $g_1(x)$ dual to the power shape function $f(y)$, cf. Eq. (27)

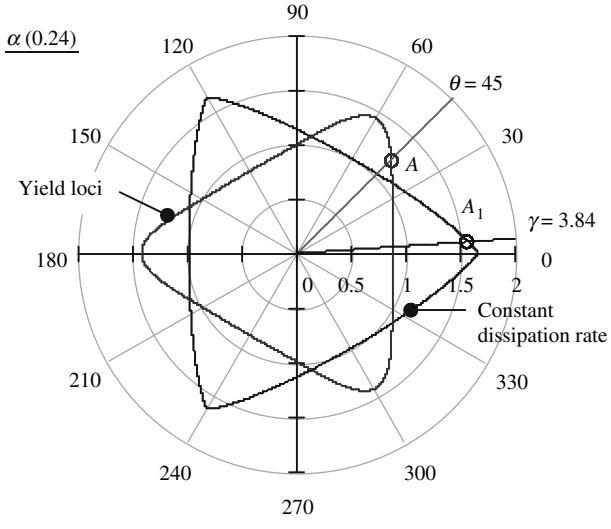


**Fig. 14.** $\pi$-Plane. Loci of dual potentials associated with power yield functions, $q_{\min} \simeq 0.609$, $n = 0.24$, $b = \alpha(0.24) = 0.775$

## Appendix A: Convexity condition

Introduce a Cartesian a coordinate system $x_1 - x_2$ on the octahedral plane. The mutual position of the $x_1$, $x_2$ axes and images of the principal stress axes are shown in Fig. 2a. The polar coordinates $r - \theta$ on the same plane are defined by the usual formulas

$$x_1 = -r\cos(\theta), \quad x_2 = r\sin(\theta). \tag{A1}$$

Let $x_1 = w(x_2)$ be a non-positive continuous and continuously differentiable function describing the curve representing the critical condition in the segment $0 \le \theta \le \pi/3$. Equivalently, the same segment of curve can be described in polar coordinates or in parametric form as

$$r = R_2(\theta) \quad \text{or} \quad x_1(\theta) = R_2(\theta)\cos(\theta), \quad x_2(\theta) = -R_2(\theta)\sin(\theta). \tag{A2}$$

Assume for simplicity the following boundary values [they are relevant for scale (14) of the shape function]:

$$R_2(\theta = 0) = 1, \quad R_2(\theta = \pi/3) = 1/q \;\Leftrightarrow\; w(0) = -1, \;\; w(a) = -0.5/q, \quad a \equiv 0.5\sqrt{3}/q \tag{A3}$$

such that the considered segment in Cartesian coordinates is $0 \le x_2 \le a$. As it is well known the images of the principal stresses on the octahedral plane shown in Fig. 2a are the symmetry axis of the whole figure enclosed by the geometrical loci of critical condition. Hence, in order no corners of the closed curve to occur at boundary points of each segment it is necessary that

$$\left.\frac{dw}{dx_2}\right|_{x_2=0} = 0, \quad \left.\frac{dw}{dx_2}\right|_{x_2=a} = \sqrt{3} \;\Leftrightarrow\; R_2'(\theta = 0) = 0, \quad R_2'(\theta = \pi/3) = 0. \tag{A4.1–4}$$

Here we restrict our discussion to the regular critical condition for which Eq. (A4) holds. Assume additionally that function $w(x_2)$ is convex in $0 \le x_2 \le a$. Then directly from the definition of convex functions we have

$$0 \le \frac{dw(x_2)}{dx_2} \le \frac{w(a) - w(x_2)}{a - x_2} \le \sqrt{3} \tag{A5}$$

on account of Eq. (A4). Since

$$x_1'(\theta) = -R_2'(\theta)\cos(\theta) + R_2\sin(\theta), \quad x_2'(\theta) = R_2'(\theta)\sin(\theta) + R_2\cos(\theta) \tag{A6}$$

the inequality (A5) implies the obvious mathematical property

$$x_2'(\theta) \ge 0, \quad x_1'(\theta) \ge 0. \tag{A7.1, 2}$$

The known differential condition of convexity of the function $w(x_2)$ can be written in the form

$$\frac{d^2w(x_2)}{dx_2^2} \ge 0 \;\Leftrightarrow\; x_2'(\theta)\frac{d}{d\theta}\left[\frac{x_1'(\theta)}{x_2'(\theta)}\right] \ge 0 \tag{A8.1, 2}$$

on account of Eq. (A7.1). Substitute Eq. (A6) into (A8.2) and perform the indicated operations to get

$$\frac{1}{R_2^2}[x_1'(\theta)]^3\frac{d^2w}{dx_2^2} = -\frac{R_2''(\theta)}{R_2} + 2\left[\frac{R_2'(\theta)}{R_2}\right]^2 + 1 \ge 0. \tag{A9}$$

Define the shape function $f_2(y)$, $y = \cos(3\theta)$ by [cf. Eqs. (14.2) and (A3)]

$$R_2(\theta) = \frac{1}{f_2[\cos(3\theta)]}, \quad -1 \le y \le 1, \quad f_2(1) = 1, \quad f_2(-1) = q. \tag{A10}$$

Substitute Eq. (A10) into Eq. (A9) and make the required differentiation to get the final result

$$(1 - y^2)f_2''(y) - yf_2'(y) + \frac{f_2(y)}{9} \ge 0. \tag{A11}$$

The condition is invariant under the change of scale of the shape function. Note that conditions (A4.3,4) will be satisfied if $f_2'(-1)$ and $f_2'(1)$ are bounded.

## Appendix B: The form of inverse relations

(i) To prove the statements (50), (51) and equivalence of Eqs. (46.1) and (57) [we will show that Eq. (57) implies Eq. (46.1)] it is expedient to perform first some algebraic manipulations upon Eqs. (41.1) and (44). The Cayley–Hamilton relations (8) and (5.2) imply

$$\boldsymbol{N}^3 = \frac{1}{2}\boldsymbol{N} + \frac{y}{3\sqrt{6}}\boldsymbol{1} \quad \Rightarrow \quad \boldsymbol{N}^4 = \frac{1}{2}\boldsymbol{N}^2 + \frac{y}{3\sqrt{6}}\boldsymbol{N}. \tag{B1}$$

Multiplication of (41.1) by $\boldsymbol{N}$, $\boldsymbol{N}^\perp$, $(\boldsymbol{N}^\perp)^2$ and $\boldsymbol{N}^2$, with use of Eq. (B1) results in

$$\sqrt{1-y^2}\boldsymbol{N}^\perp\boldsymbol{N} = -y\boldsymbol{N}^2 + \frac{\sqrt{6}}{6}\boldsymbol{N} + \frac{y}{3}\boldsymbol{1}, \tag{B2}$$

$$(\boldsymbol{N}^\perp)^2 = \frac{2}{3}\boldsymbol{1} - \boldsymbol{N}^2, \quad \sqrt{1-y^2}(\boldsymbol{N}^\perp)^3 = \frac{\sqrt{6}}{2}\boldsymbol{N}^2 - \frac{3}{2}y\boldsymbol{N} - \frac{\sqrt{6}}{18}(4-y^2)\boldsymbol{1}, \tag{B3.1, 2}$$

$$(\boldsymbol{N}^\perp)^2\boldsymbol{N} = \frac{1}{6}\boldsymbol{N} - \frac{y}{3\sqrt{6}}\boldsymbol{1}, \quad \sqrt{1-y^2}\boldsymbol{N}^\perp\boldsymbol{N}^2 = \frac{\sqrt{6}}{6}\boldsymbol{N}^2 - \frac{y}{6}\boldsymbol{N} - \frac{y^2}{3\sqrt{6}}\boldsymbol{1}. \tag{B4}$$

Hence

$$\begin{aligned} &-\sqrt{6}\,tr[(\boldsymbol{N}^\perp)^3] = \sqrt{6}\,\mathrm{tr}(\boldsymbol{N}^\perp\boldsymbol{N}^2) = \sqrt{1-y^2} = \sin(3\theta), \\ &-\sqrt{6}\,tr[(\boldsymbol{N}^\perp)^2\boldsymbol{N}] = \sqrt{6}\,\mathrm{tr}(\boldsymbol{N}^3) = -\sqrt{6}\,\mathrm{tr}[(\boldsymbol{N}^\perp)^2\boldsymbol{N}] = y = \cos(3\theta), \end{aligned} \tag{B5}$$

and obviously $\mathrm{tr}[(\boldsymbol{N}^\perp)^2] = 1$ . Multiplication of Eq. (44) by $\boldsymbol{n}$ and $\boldsymbol{n}^2$ gives

$$\begin{aligned} &\boldsymbol{n}^2 = A^2\boldsymbol{N}^2 + 2AB\boldsymbol{N}\boldsymbol{N}^\perp + B^2(\boldsymbol{N}^\perp)^2, \\ &\boldsymbol{n}^3 = A^3\boldsymbol{N}^3 + 3A^2B\boldsymbol{N}^2\boldsymbol{N}^\perp + 3B^2A(\boldsymbol{N}^\perp)^2\boldsymbol{N} + B^3(\boldsymbol{N}^\perp)^3. \end{aligned} \tag{B6.1, 2}$$

(ii) The result (50), (51) follows from (B6.2). Calculate the trace of the Eq. (B6.2) and use of Eq. (B5) to get

$$x = \sqrt{6}\mathrm{tr}(\boldsymbol{n}^3) = y(A^3 - 3B^2A) + \sqrt{1-y^2}(3A^2B - B^3) \tag{B7}$$

or equivalently

$$x = \cos(3\gamma) = \cos(3\theta)\cos(3\chi) + j^*\sin(3\theta)\sin(3\chi) = \cos[3(\theta - j^*\chi)]$$

on account of Eqs. (5.2) and (45). This is the proof of relations (50) and (51).

(iii) To justify Eq. (53) calculate the total differential of Eq. (52) and write it in the following form:

$$\frac{g'(x)}{g(x)}dx = \frac{A'(y)}{A(y)}dy - \frac{f'(y)}{f(y)}dy. \tag{B8}$$

Note that $A'(y)dy + j^*Bd\chi = 0$, $\quad (A(y) = \cos(\chi),\ B = j^*\sin(\chi))$ which implies

$$\frac{A'(y)}{A(y)}dy + 3\sqrt{1-y^2}\frac{f'(y)}{f(y)}j^*d\chi = 0 \tag{B9}$$

on account of (45.2). Since $y = \cos(3\theta) \Rightarrow dy = -3\sqrt{1-y^2}d\theta$ and likewise $x = \cos(3\gamma) \Rightarrow dx = -3\sqrt{1-x^2}d\gamma$, the total differential of the relation $\theta = \gamma + j^*\chi$, cf. Eq. (51.2), is

$$j^*d\chi = \frac{dx}{3\sqrt{1-x^2}} - \frac{dy}{3\sqrt{1-y^2}}. \tag{B10}$$

Eliminate in turn $j^*\,d\chi$ between Eqs. (B9) and (B10), and then $A'(y)dy/A(y)$ from the resulting equation and Eq. (B8) to get Eq. (53).

(iv) To show that Eq. (57.1) implies Eq. (46.1) express $\boldsymbol{n}^2 - \boldsymbol{1}/3$ in terms of $\boldsymbol{N}$ and $\boldsymbol{N}^\perp$ . To this end solve Eq. (41.1) with respect to $\boldsymbol{N}^2$,

$$\sqrt{6}\boldsymbol{N}^2 = y\boldsymbol{N} + \sqrt{1-y^2}\boldsymbol{N}^{\perp} + \boldsymbol{1}(\sqrt{6}/3), \tag{B11}$$

and substitute this result into Eqs. (B2) and (B3.1),

$$\sqrt{6}\boldsymbol{N}^{\perp}\boldsymbol{N} = \sqrt{1-y^2}\boldsymbol{N} - y\boldsymbol{N}^{\perp}, \quad \sqrt{6}\,(\boldsymbol{N}^{\perp})^2 = \frac{\sqrt{6}}{3}\boldsymbol{1} - y\boldsymbol{N} - \sqrt{1-y^2}\boldsymbol{N}^{\perp}. \tag{B12}$$

Substitute Eqs. (B12) and (B11) into Eq. (B6.1), and find the following decomposition:

$$\sqrt{6}\left(\boldsymbol{n}^2 - \frac{1}{3}\boldsymbol{1}\right) = \left[(A^2-B^2)y + 2AB\sqrt{1-y^2}\right]\boldsymbol{N} + \left[(A^2-B^2)\sqrt{1-y^2} - 2ABy\right]\boldsymbol{N}^{\perp} \tag{B13}$$

which together with Eq. (44) enables to write Eq. (57) in the following form:

$$\sqrt{1-x^2}\boldsymbol{n}^{\perp} = \left[(A^2-B^2)y + 2AB\sqrt{1-y^2} - Ax\right]\boldsymbol{N} + \left[(A^2-B^2)\sqrt{1-y^2} - 2ABy - Bx\right]\boldsymbol{N}^{\perp}. \tag{B14}$$

However, for dual couple, the relation (51.2) (proved above) implies

$$\cos(3\gamma + j^*\chi) = \cos(3\theta - 2j^*\chi) \;\Rightarrow\; (A^2-B^2)y + 2AB\sqrt{1-y^2} = Ax - B\sqrt{1-x^2}, \tag{B15}$$

$$\sin(3\gamma + j^*\chi) = \sin(3\theta - 2j^*\chi) \;\Rightarrow\; (A^2-B^2)\sqrt{1-y^2} - 2ABy = Bx + A\sqrt{1-x^2}. \tag{B16}$$

When this is combined with Eq. (B14) one finally gets

$$\boldsymbol{n}^{\perp} = -B\boldsymbol{N} + A\boldsymbol{N}^{\perp}$$

and thus proves that Eq. (57) implies Eq. (46.1).

## References


[1] Spitzig, R.J., Richmond, O.: The effect of pressure on the flow stress of metals. Acta Metall. **32**, 457–463 (1984)

[2] Chait, R.: Factors influencing the strength differential of high strength steels. Metall. Trans. **3**, 365 (1972)

[3] Chait, R.: The strength differential of steel and Ti alloys as influenced by test temperature and microstructure. Scr. Metall. **7**, 351 (1973)

[4] Casey, J., Sullivan, T.D.: Pressure dependency strength differential effect and plastic volume expansion in metals. Int. J. Plast. **1**, 39 (1985)

[5] Rauch, G.C., Leslie, W.C.: The extent and nature of the strength differential effects in steels. Metall. Trans. **3**, 373 (1972)

[6] Kuroda, M., Kuwabara, T.: Shear band development in polycrystalline metal with strength-differential effect and plastic volume expansion. Proc. R. Soc. Lond. A **458**, 2243–2262 (2002)

[7] Hosford, W.F., Allen, T.J.: Twinning and directional slip as a cause for strength differential effect. Met. Trans. **4**, 1424–1425 (1973)

[8] Hosford, W.F.: The Mechanics of Crystals and Textured Polycrystals. Oxford University Press, New York (1993)

[9] Raniecki, B., Lexcellent, C.: Thermodynamics of isotropic pseudoelasticity in shape memory alloys. Eur. J. Mech. A/Solids **17**, 186–205 (1998)

[10] Lexcellent, C., Vivet, A., Bouvet, C., Calloch, S., Blanc, P.: Experimental and numerical determinations of the initial surface of phase transition under biaxial loading in some polycrystalline shape-memory alloys. J. Mech. Phys. Solids **50**, 2717–2735 (2002)

[11] Huang, W.: Yield surfaces of shape memory alloys and their applications. Acta Mater. **47**, 2769–2776 (1999)

[12] Iyer, S.K., Lissenden, C.J.: Multiaxial constitutive model accounting for the strength-differential in Inconnel 718. Int. J. Plast. **19**, 2055–2081 (2003)

[13] Casacu, O., Barlat, F.: A criterion for description of anisotropy and yield differential effects in pressure-insensitive materials. Int. J. Plast. **20**, 2027–2045 (2004)
[14] Shrivastawa, H.P., Mróz, Z, Dubey, R.N.: Yield criterion and the hardening rule for a plastic solid. Zeitschr. Angew. Math. Mech. (ZAMM) **53**, 625–633 (1973)
[15] Drucker, D.C.: Relation of experiments to mathematical theories of plasticity. J.Appl. Mech. **16**, 349–357 (1949)
[16] Hill, R.: On intrinsic eigenstates in plasticity with generalized variables. Math. Proc. Camb. Philos. Soc. **93**, 177–189 (1983)
[17] Podgórski, J.: Limit state condition and the dissipation function for isotropic materials. Arch. Mech. **36**, 323–342 (1984)
[18] Podgórski, J.: General failure criterion for isotropic media. J. Engng. Mech. ASCE **111**(2), 188–199 (1985)
[19] Lade, P.V., Duncan, J.M.: Elastoplastic stress-strain theory for cohesionless soil. J. Geotech. Eng. Div. ASCE, 101, GT10, Proc. Paper 11670, 1037–1053 (1975)
[20] Matsuoka, H.: On the significance of the spatial mobilized plane. Soil and Found., 16, 1, Jap. Soc. Soil Mech. Found. Engng., March 1976
[21] Ottosen, N.S.: A failure criterion for concrete. J. Engng. Mech., ASCE, 103, EM4, Proc. Paper 13111, 527–535 (1977)
[22] Raniecki, B., Tanaka, K., Ziółkowski, A.: Testing and modeling NiTi SMA at complex stress state-Selected results of Polish–Japanese research cooperation. Material Sci. Research International, Special Technical Publication **2**, 327–334 (2001)
[23] Mills, L.L., Zimmerman, R.M.: Compressive strength of plain concrete under multiaxial loading conditions. J. ACI. Proc. **V67**, 10 (1970)
[24] Gudehus, G.: Elastoplastische Stoffgleichungen für trockenen Sand. Ing. Archiv **42**, 3 (1973)